

DELAYED-MUTUAL COUPLING DYNAMICS OF LASERS: SCALING LAWS AND RESONANCES

T.W. CARR ^{*}, I.B. SCHWARTZ [†], MIN-YOUNG KIM [‡], AND RAJARSHI ROY [§]

Abstract. We consider a model for two lasers that are mutually coupled optoelectronically by modulating the pump of one laser with the intensity deviations of the other. Signal propagation time in the optoelectronic loop causes a significant delay leading to the onset of oscillatory output. Multiscale perturbation methods are used to describe the amplitude and period of oscillations as a function of the coupling strength and delay time. For weak coupling the oscillations have the laser's relaxation period, and the amplitude varies as the one-fourth power of the parameter deviations from the bifurcation point. For order-one coupling strength the period is determined as multiples of the delay time, and the amplitude varies with a square-root power law. Because we allow for independent control of the individual coupling constants, for certain parameter values there is an atypical amplitude-resonance phenomena. Finally, our theoretical results are consistent with recent experimental observations when the inclusion of a low-pass filter in the coupling loop is taken into account.

Key words. coupled lasers, delay, Hopf bifurcation, resonance

AMS subject classifications. 34D15, 37G15, 39A11, 78A60

1. Introduction. In recent work, we presented experimental and simulation results for two mutually coupled lasers [1] with time-delayed asymmetric coupling. The light emitted from one laser propagates through fiber-optic cables to a photodetector that generates an electronic signal proportional to the light-intensity deviations from steady state. The electronic signal may be attenuated or amplified before it modulates the pump current of the other laser. The propagation time of the signal in the optoelectronic path introduces a significant time delay, and the coupling strength in each direction can be controlled separately. Our work in [1] investigated how the time delay and asymmetric coupling led to oscillatory and pulsating laser output. In this paper, we present a more theoretical exploration of the dynamics that result from this coupling configuration.

In [2] we investigated this same configuration (asymmetric pump coupling) but without including the effect of delay. In addition, the coupling constant from laser-2 to laser-1 was negative, while the coupling constant from laser-1 to laser-2 was positive. That is, we assumed that the electronic coupling signal from laser-2 was inverted before applying it to the pump of laser-1. For purely harmonic signals, having opposite-sign coupling constants is equivalent to time-delayed coupling when the delay is half of the period. We found that as the coupling constant from laser-2 to laser-1 is increased in magnitude: (i) There is a Hopf bifurcation to oscillatory output. (ii) For certain parameter values there exists a small-coupling resonance such that the amplitudes of both lasers are pulsating. (iii) For large coupling, laser-2 acts as a small-amplitude, nearly harmonic modulation to laser-1. Laser-1 exhibits period-doubling bifurcations to chaos and complex subharmonic resonances.

^{*} Department of Mathematics, Southern Methodist University, Dallas, TX 75275-0156, tel: 214-768-3460, tcarr@smu.edu

[†] Nonlinear Dynamical Systems Section, Code 6792, Naval Research Laboratory, Washington, DC 20375, tel: 202-404-8359, schwartz@nlschaos.nrl.navy.mil

[‡] Department of Physics, University of Maryland, College Park, MD, 20742, tel: 514-398-8224, mmykim@cnd.mcgill.ca

[§] Department of Physics, University of Maryland, College Park, MD, 20742, rroy@glue.umd.edu

In this paper we include the effect of the delayed-coupling, which results in a coupled set of delay-differential equations (DDEs). With delay there is again a Hopf bifurcation to oscillatory output. However, the delay allows for periodic oscillations not just at the laser’s relaxation period as in [2], but at periods that are integer multiples of the delay; we refer to the former oscillatory solutions as “internal modes,” and the latter as “external modes.” We show that as the coupling strength is increased, the first instability is a Hopf bifurcation to the internal mode. Our nonlinear analysis then shows that the amplitude of the internal mode varies as the one-fourth root of the bifurcation parameter’s deviation from the Hopf bifurcation point.

However, in the experiments of [1] the output was not the internal mode but an external mode. The period of the oscillatory output was a multiple of the delay, and the amplitude of the oscillations varied as the square root of the bifurcation parameter. The discrepancy is due to the fact that the optoelectronic coupling contains an intrinsic low-pass filter that attenuates the internal mode. We show that the filter selects the external mode with the greatest possible frequency passed by the low-pass filter. A nonlinear analysis then shows that the amplitude of the external modes does indeed vary with a square-root power law.

For the coupled lasers without delay in [1], we found that the parameters could be tuned to cause a resonance-type effect with respect to the coupling; more specifically, the coupling could be tuned to maximize the amplitude of the oscillatory output. We find that this resonance effect also occurs with the inclusion of the delay. However, there are some dramatic qualitative differences as the coupling parameters are varied. In the system with delay, the branch of periodic solutions in the bifurcation diagram can be smoothly folded to form parameter intervals of bi-stability. Then there is a critical value of the same coupling parameter beyond which the bi-stability disappears suddenly and non-smoothly.

Our coupling scheme is an example of “incoherent coupling” [3] because it depends only on the laser’s intensity and not on the complex electric field. This is because the intensity of one laser affects the other only indirectly; in our case, the intensity of one laser modulates the pump current of the other. In contrast, “coherent coupling” refers to when the optical field of one laser is directly injected into the cavity of the other laser. Analogously, a single laser with delayed and re-injected self-feedback would be called “coherent” feedback. Semiconductor lasers with delayed coherent feedback have been extensively studied because of their widespread application in electronics and communication systems; there the laser’s output signal may be reflected off external surfaces back into the laser. The Lang-Kobayashi DDEs [4] are the canonical model for semiconductor lasers with delayed self-feedback and have been used to investigate phenomena ranging from the onset of instabilities to the development of chaotic output referred to as “coherence collapse” (see [5] for a review). Coupled sets of Lang-Kobayashi or related DDEs are most often used to describe coherently-coupled semiconductor lasers with delay. Two recent studies [6, 7] are in the same spirit as this paper as they track the number of and properties of oscillatory solutions that appear as the coupling strength is increased.

The main simplification that results from considering incoherent coupling between the lasers is that neither the laser-frequency detuning nor the electric-field phase differences affect the dynamics of the coupled system [8]. Pieroux et al. [9] have shown that the electrooptical coupling we consider in this paper leads to an equivalent dynamical model as incoherent coupling. There have recently been a number of other investigations of lasers with incoherent coupling. The main focus of many of these

works was on chaotic synchronization (see [10] and included references). Two recent papers by Vicente et al. [11, 12] consider a similar implementation of optoelectronic coupling to that we consider here, i.e., the intensity of one laser modulates the pump current of the other. Their investigation of the oscillatory solutions is mainly numerical and they discuss interesting phenomena such as amplitude quenching, frequency locking and routes to chaos.

Delay-coupled relaxation and limit-cycle oscillators have been the subject of many investigations (see [13, 14, 15, 16, 17, 18] and their included references). These systems are self-oscillatory and the amplitude is often fixed by the intrinsic properties of the oscillator. In many cases the system may be reduced to a phase equation, or a system of phase equations if the oscillators are coupled [19].

In contrast, for laser systems the amplitude is an important dynamical variable. This is because the lasers we consider are weakly damped, nearly conservative systems such that the steady state is the only asymptotically stable solution. Oscillations must be induced by external mechanisms such as modulation, injection or coupling [20]. Thus, the amplitude of the oscillations is highly dependent upon the external mechanism, in our case the coupling, rather than the individual laser. We should mention that for coupled limit-cycle oscillators there is the amplitude instability referred to as “amplitude death,” where for specific values of the coupling (and oscillator parameter values) the amplitude becomes zero.

After presenting our model, we show that the linear-stability analysis predicts a critical value of the coupling constant (that depends upon the delay time) such that there is Hopf bifurcation to the internal mode, i.e., oscillations with the intrinsic relaxation period. We then use multiple-scale perturbation methods, modified to account for time delays [21], to analyze the long-time evolution of the internal mode. The results are a pair of complex Stuart-Landau DDEs for the oscillation amplitudes that include a slow-time delay term. We analyze the amplitude equations to determine the bifurcation properties of the internal mode. Of particular note is that we allow for independent control of the coupling constants; most other studies of coupled lasers and oscillators consider symmetric coupling, where the coupling is the same across all of the elements. The independent control is important because, as we will show, it allows for a singularity in the bifurcation equations that marks the “resonance” of large amplitude solutions.

The Hopf bifurcation to the internal mode occurs for small coupling. However, as the coupling is increased, the external modes appear via Hopf bifurcations. We have extended our multiple-scale analysis to be able to describe the bifurcation of the external modes that occur for $O(1)$ coupling. The analytical challenge is that the delay terms remain a part of the leading-order problem. Describing the bifurcation of the external modes is important for comparing our results to those in experiments [22], because the experimental system contains low-pass filters that attenuate the internal mode originating from the first Hopf bifurcation.

An alternative to our multiple-scale method for deriving slow-time amplitude equations is to apply center-manifold theory with averaging [23, 14, 15]. However, the averaging method does not retain the delay in the slow time; that is, the amplitude equations are ordinary-differential equations, not DDEs. The distinction is not important for their or our investigation because we look for steady-state solutions of the amplitude equations. However, time-varying amplitudes may require consideration of the slow-time delay.

Reddy et al. [16, 24] considered delay-coupled Stuart-Landau DDEs similar to

the amplitude equations we derive here. However, the complex coefficients they use are appropriate for limit-cycle oscillators and not the lasers that we consider. They focus their work on the properties of synchronization and amplitude death.

In the next section, we nondimensionalize the model for two-coupled lasers, with the result being the focus of the rest of the paper. We perform the linear-stability analysis in Sec. 3. Slow-time evolution equations for small and $O(1)$ coupling are derived in Sec. 4 and Sec. 5, respectively. We close with a discussion of the results.

2. Class-B model. We consider two class-B lasers [20, 25] modeled by rate equations as

$$(2.1) \quad \begin{aligned} \frac{dI_j}{dt} &= (D_j - 1)I_j, \quad j = 1, 2 \\ \frac{dD_j}{dt} &= \epsilon_j^2 [A_j(t) - (1 + I_j)D_j], \end{aligned}$$

where I_j and D_j are the scaled intensity and population inversion, respectively, of each laser. Scaled time t is measured with respect to the cavity-decay constant κ , $t = (2\kappa)t_r$, where t_r measures real time. $\epsilon^2 = \gamma_{\parallel}/(2\kappa)$ is a ratio of the inversion-decay rate, γ_{\parallel} , to the cavity-decay rate, κ , and measures the relative life-time of photons to excited electrons. $A(t)$ is the dimensionless pump rate and corresponds to the energy input to the laser by an external source, e.g., another laser, an incoherent light source or an electronic current. The mass-action coupling term ID models “stimulated emission”; a photon passing through the laser cavity stimulates an excited electron to drop to the lower energy level, resulting in one less excited electron and one more photon. Eqs. (2.1) may be derived as a reduced model from semi-classical Maxwell-Bloch equations [20, 25, 26]; the latter use Maxwell’s equations to describe the laser’s electromagnetic fields coupled with the Bloch equations from quantum mechanics for the amplifying media.

If the pump rate is a constant, $A_j(t) = A_{j0}$, then the laser relaxes to the steady state $D_{j0} = 1$, $I_{j0} = A_{j0} - 1$. To facilitate further analysis, we define new variables for the deviations from the non-zero steady state [27] as

$$(2.2) \quad I_j = I_{j0}(1 + y_j), \quad D_j = 1 + \epsilon_j \sqrt{I_{j0}} x_j, \quad s = \epsilon_1 \sqrt{I_{10}} t.$$

Our goal is to investigate the effects of coupling through the pump. In addition, we account for the effect of a delay when the signal from one laser takes a non-negligible time before affecting the other. Thus, the pump coupling is taken to be

$$(2.3) \quad A_j(t) = A_{j0} - I_{j0} \delta_k y_k(t - \tau_k).$$

Thus, we feed the intensity *deviations* $y_k = (I_k - I_{k0})/I_{k0}$ from the steady-state output of laser k to the pump of laser j ; the strength of the coupling is controlled by δ_k . The pump-coupling scheme allows for easy electronic control of the coupling signal. The negative coupling results from the configuration of the electronic coupling circuits in [1]. Finally, we assume that the decay constants of the two lasers are related by $\epsilon_2 = \epsilon_1 \frac{\sqrt{I_{10}}}{\sqrt{I_{20}}} \beta$. The new rescaled equations are

$$\begin{aligned} \frac{dy_1}{dt} &= x_1(1 + y_1), \\ \frac{dx_1}{dt} &= -y_1 - \epsilon x_1(a_1 + by_1) - \delta_2 y_2(t - \tau_2), \end{aligned}$$

$$(2.4) \quad \begin{aligned} \frac{dy_2}{dt} &= \beta x_2(1 + y_2), \\ \frac{dx_2}{dt} &= \beta[-y_2 - \epsilon\beta x_2(a_2 + by_2) - \delta_1 y_1(t - \tau_1)], \end{aligned}$$

where

$$(2.5) \quad a_1 = \frac{1 + I_{10}}{\sqrt{I_{10}}}, \quad a_2 = \frac{\sqrt{I_{10}}(1 + I_{20})}{I_{20}}, \quad \text{and } b = \sqrt{I_{10}}.$$

For notational convenience we have let $s \rightarrow t$ and dropped the subscript on ϵ_1 ($\epsilon_1 \rightarrow \epsilon$). Register et al. [28] have considered a very similar model to ours; however, in their case the cross-coupling term is instantaneous, while the delay appears through self-feedback of each laser's own intensity.

3. Linear stability of the steady state.

3.1. Characteristic equation. In the new variables, the steady state is given by $x_j = y_j = 0$. The linear stability of the steady state is determined by studying the evolution of small perturbations, for which we obtain the characteristic equation

$$(3.1) \quad [\lambda(\lambda + \epsilon a_1) + 1][\lambda(\lambda + \epsilon a_2 \beta^2) + \beta^2] - \beta^2 \delta_1 \delta_2 e^{-\lambda(\tau_1 + \tau_2)} = 0.$$

The delay results in the exponential term $\exp(-\lambda(\tau_1 + \tau_2))$. The transcendental form of the characteristic equation and, hence, the possibility of an infinite number of roots is typical for DDEs.

If either $\delta_j = 0$, then there are only decaying oscillations, which indicates that a single uncoupled laser is a weakly damped oscillator; this is the general characteristic of “class-B” lasers [25]. For $\delta_j \neq 0$ numerical simulations indicate there is a Hopf bifurcation as the δ_j are increased. To identify the Hopf bifurcation point, we let $\lambda = i\omega$ and separate the characteristic equation into real and imaginary parts. After some algebra we obtain a single equation for the frequency and another equation for the value of $\Delta = \delta_1 \delta_2$ at the bifurcation point. The equations are

$$(3.2) \quad \begin{aligned} 0 &= \tan(\omega\tau_s)[(1 - \omega^2)(\beta^2 - \omega^2) - \epsilon^2 a_1 a_2 \beta^2 \omega^2] \\ &\quad + \epsilon\omega(1 - \omega^2)(a_1 + a_2 \beta^2), \end{aligned}$$

$$(3.3) \quad \begin{aligned} \beta^2 \Delta_H^2 &= [(1 - \omega^2)(\beta^2 - \omega^2) \\ &\quad - \epsilon^2 a_1 a_2 \beta^2 \omega^2]^2 + [\epsilon\omega(1 - \omega^2)(a_1 + a_2 \beta^2)]^2, \end{aligned}$$

where $\tau_s = \tau_1 + \tau_2$ is the “round-trip” delay time. The transcendental equation for ω can be solved numerically and its solution is then substituted into Eq. (3.3) to determine the value of the coupling at the bifurcation point $\Delta = \Delta_H$.

To simplify further discussion we consider $\beta = 1$. This implies $\epsilon_2 = \epsilon_1 \sqrt{I_{10}/I_{20}}$, which is a specific relationship between the lasers' decay constants, $\gamma_{\parallel,j}$ and κ_j , and the pump rate, $A_j 0$; if $\beta = 1$ and $A_{10} = A_{20}$ then the lasers are identical. The results are qualitatively the same for nearly identical lasers with $\beta \approx 1$. To simplify notation, we define $c_1 = a_1 + a_2$ and $c_2 = a_1 a_2$ and have

$$(3.4) \quad 0 = \tan(\omega\tau_s)[(1 - \omega^2)^2 - \epsilon^2 c_2 \omega^2] + \epsilon\omega(1 - \omega^2)c_1,$$

$$(3.5) \quad \Delta_H^2 = [(1 - \omega^2)^2 - \epsilon^2 c_2 \omega^2]^2 + [\epsilon\omega(1 - \omega^2)c_1]^2,$$

For $\epsilon \ll 1$ the leading approximation to the frequency is given by $\omega = \pm 1$ or $\omega = m\pi/\tau_s$, m an integer. We will refer to the former as the *internal mode* because

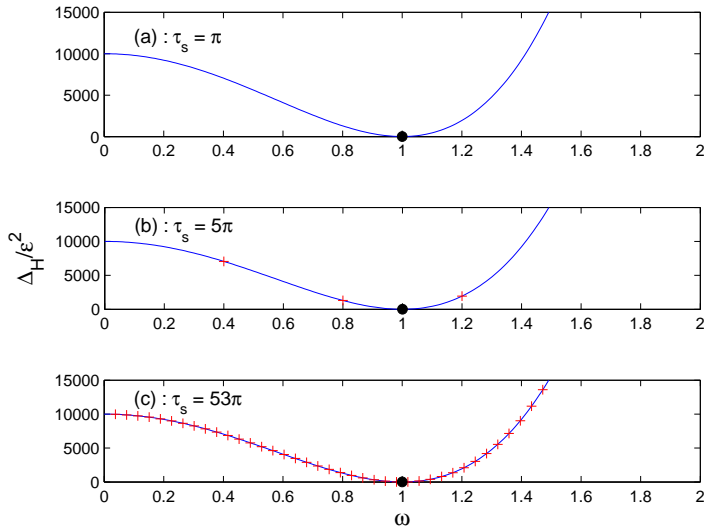


FIG. 3.1. Neutral stability curve $\Delta_H(\omega)$ (solid curve) for Hopf bifurcations described by Eq. (3.5). The solid circle at $\omega \approx 1$ indicates the internal mode. The crosses (+) at $\omega \approx m\pi/\tau_s$ indicate the external modes. Because $\tau_s = n\pi$, then $\omega \approx m/n$ for the external modes. ($\epsilon = 0.01, a_1 = a_2 = 2, b = 1, \beta = 1$)

this is the scaled laser-relaxation frequency; more specifically, an oscillatory solution of Eq. (2.4) with period $\omega = 1$ is called the internal mode. Similarly, oscillatory solutions with period $\omega = m\pi/\tau_s$, m an integer, are called *external modes* because their periods are determined by the delay. For any fixed value of the delay τ_s there is the internal mode and an infinite number of external modes.

From Eq. (3.5) we see that for almost all values of the delay, as the coupling is increased from zero, the bifurcation to the internal mode occurs at a lower value of the Δ_H than the external mode (this is true except when $\tau_s = n\pi$, n even, which we will discuss in later paragraphs). More specifically, for the internal mode with $\omega \approx 1$ the Hopf bifurcation occurs when $\Delta_H = O(\epsilon^2) \ll 1$. For the external mode with $\omega = O(1)$ the value of the coupling at the Hopf bifurcation is $\Delta_H = O(1)$. This is illustrated in Fig. 3.1, where we have plotted Eq. (3.5). We will determine more precise approximations for these bifurcation points below; however, we will first make additional qualitative observations.

Let us fix the delay to be a multiple of π , i.e., $\tau_s = n\pi$, n an integer. Then $\omega = \pm 1$, corresponding to the internal mode, is an exact solution to the frequency equation Eq. (3.4) and $\Delta_H = \pm\epsilon^2 c_2$. The + is taken if n is odd and the - is taken if n is even (the sign association comes from the real and imaginary parts of the characteristic equation before ω and Δ were separated). In the present paper, we will consider $\delta_j > 0$ and $\Delta > 0$; results for $\Delta < 0$ are qualitatively the same. Thus, we have the exact solution $\omega = \pm 1$, $\Delta_H = +\epsilon^2 c_2$ when $\tau_s = n\pi$, n odd. An analysis of Eq. (3.5) shows this occurs at a minimum in the curve $\Delta_H(\omega)$ as illustrated in Fig. 3.1.

If τ_s is *not* a multiple of π , say $n\pi < \tau_s < (n+1)\pi$, the Hopf bifurcation to the internal mode still occurs before the bifurcation to any of the external modes. The frequency of the internal mode is $\omega \approx 1$ (instead of $\omega = 1$), and $\Delta_H > \epsilon^2 c_2$ but

still $O(\epsilon^2)$. Thus, if we plot Δ_H as a function of the delay τ_s , the *minimum* of the curves $\Delta_H(\tau_s)$ occur when $\tau_s = n\pi$, n odd. This is illustrated in Fig. 3.3 and will be discussed further below.

Now consider the external modes with $\omega \approx m\pi/\tau_s$. For negative couplings when $\delta_j > 0$ (see Eq. (2.3)) and $\Delta > 0$ an analysis of the characteristic equation shows that m *must be even*. Thus, the external modes have frequencies $\omega \approx 2\pi/\tau_s$, $4\pi/\tau_s$, etc. In Fig. 3.1 we illustrate three cases when $\tau_s = n\pi$, $n = 1, 5$, and 53 . The external modes then have $\omega = m/n$, m even.

Finally, we consider the case when $\tau_s = n\pi$, for n *even*. As discussed in the previous paragraph, for negative couplings the external modes with frequency $\omega = m\pi/\tau_s$ require that $m = 2, 4, 6 \dots$. Thus, for each external mode there is a value of $\tau_s = n\pi$, n even, such that $\omega \approx 1$ similar to the internal mode. This is illustrated in the numerical data of Fig. 3.3a for $\tau_s = 2\pi$, while in Fig. 3.3b we see that the bifurcations to these two modes occur at nearly the same value of the coupling. Referencing Fig. 3.1, the two modes would have frequencies on opposite sides of $\omega = 1$ such that Δ_H is the same for each. This is referred to as a “double Hopf” [21, 29] and may lead to more complicated bifurcation scenarios that we will not pursue in the present paper. We also note that at the double Hopf bifurcation, the designation of “internal mode” versus “external mode” is ambiguous because both have $\omega \approx 1$. Indeed, following the numerical data in Fig. 3.3a, as τ_s is varied through 2π , we see that $n = 1$ internal mode becomes the $m = 2$ external mode, while the $m = 2$ external mode becomes the $n = 3$ internal mode.

3.2. Approximations to internal and external modes. As discussed above, for any delay τ_s when the coupling is increased, the first periodic solutions to appear correspond to the internal mode and will have frequency $\omega \approx 1$. For arbitrary delay we can find an approximation for the frequency by letting $\omega = 1 + \epsilon\omega_1 + O(\epsilon^2)$ in Eq. (3.4) to find that ω_1 satisfies

$$(3.6) \quad \tan(\tau_s)[4\omega_1^2 - c_2] - 2c_1\omega_1 = 0,$$

which is a simple quadratic for ω_1 . The bifurcation point is then approximated as

$$(3.7) \quad \begin{aligned} \Delta_H^2 &= \epsilon^4[16\omega_1^4 + 4(c_1^2 - 2c_2)\omega_1^2 + c_2^2], \\ &= \epsilon^4(4\omega_1^2 + a_1^2)(4\omega_1^2 + a_2^2). \end{aligned}$$

We can obtain simpler results than Eqs. (3.6) and (3.7) if we require that $\tau_s \approx n\pi$, n odd; that is, in Fig. 3.2 we examine locally to the critical values $\omega(\tau_s) = 1$ and the minimum of the curves $\Delta_H(\tau_s)$. If $\tau_s = n\pi + \epsilon\tau_{s1}$, then

$$(3.8) \quad \omega = 1 - \epsilon^2 \frac{c_2}{2c_1} \tau_s + O(\epsilon^2), \quad \Delta_H^2 = \epsilon^4 c_2^2 + O(\epsilon^5).$$

For the external modes we let $\omega = \omega_0 + \epsilon\omega_1 + O(\epsilon^2)$ with $\omega_0 = m\pi/\tau_s$, m even, and find that

$$(3.9) \quad \omega = \omega_0 - \epsilon \frac{\omega_0 c_1}{(1 - \omega_0^2)\tau_s} + \dots$$

and the Hopf bifurcation point is approximated as

$$(3.10) \quad \Delta_H^2 = (1 - \omega_0^2)^4 + \epsilon \frac{8c_1}{\tau_s} (1 - \omega_0^2)^2 \omega_0^2 + \dots$$

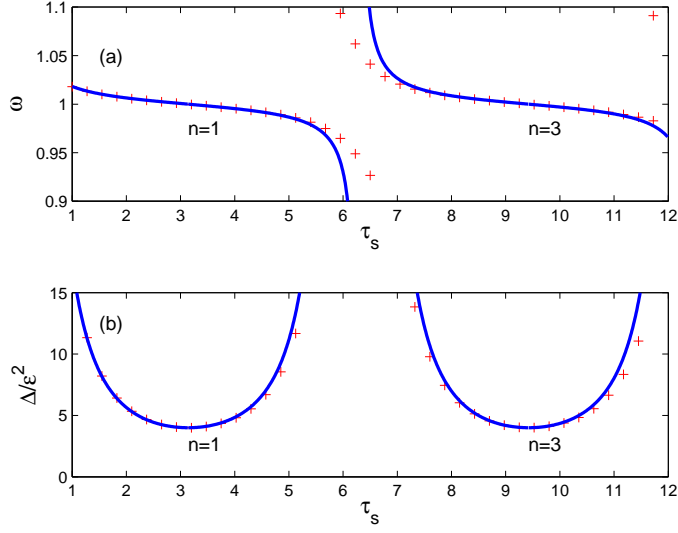


FIG. 3.2. Frequency ω and coupling $\Delta = \delta_1 \delta_2$ at the Hopf bifurcation point as a function of the delay $\tau_s = \tau_1 + \tau_2$. The solid curve is the asymptotic results of Eq. (3.6) and (3.7), while the + are the result of numerically evaluating Eq. (3.4) and (3.5). ($\epsilon = 0.01, a_1 = a_2 = 2, \beta = 1$)

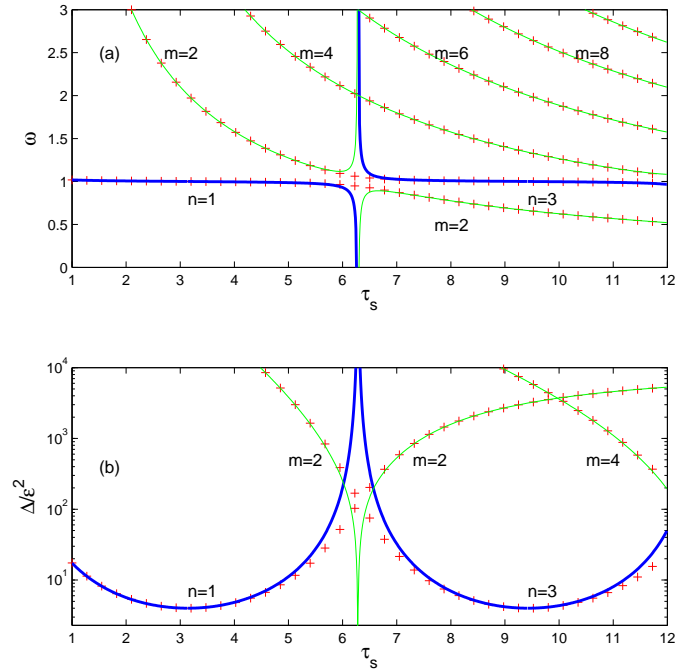


FIG. 3.3. Same as Fig. 3.2 but with a wider range in ω and Δ . The + indicate the numerical results. The thick curves are the analytical approximations of the internal modes (same as Fig. 3.2). The thin curves are the approximations of the external modes.

The external mode results are valid for τ_s such that $\omega_0 \neq 1$; thus, τ_s must be away from the double Hopf point when $\tau_s = m\pi$.

In Figs. 3.2 and 3.3 we plot the linear stability given by: (i) numerically evaluating Eqs. (3.4) and (3.5) (marked with +) and (ii) the asymptotic approximations from Eqs. (3.6)-(3.7) and Eqs. (3.9)-(3.10) (solid curves). Fig. 3.2 focuses on the bifurcation of the internal mode. For any fixed value of the delay time τ_s , we increase Δ until the curve is crossed at $\Delta = \Delta_H$; the frequency is $\omega \approx 1$. In Fig. 3.3 we pan out so that both the internal and external modes are visible. From here we see that as Δ is increased, the bifurcation to the internal mode always occurs first. As Δ is increased further, we cross secondary curves indicating the bifurcations to the external modes. More specifically, suppose that $\tau = \pi$ ($n = 1$). After the internal mode, the external modes with frequencies $\omega = m/n = m/1$, $m = 2, 4, \dots$ appear in sequence. For longer delay times, the order in which the external modes appear will be different; this can be seen in Fig. 3.3 for $\tau_s \approx 11$, where the bifurcation to the external mode with $m = 4$ occurs before the mode with $m = 2$. Alternatively, in Fig. 3.1b when $\tau_s = 5\pi$, as Δ is increased the bifurcation to the periodic solutions occur in the order $\omega \approx 1$, ≈ 0.8 , ≈ 1.2 , ≈ 0.4 , which corresponds to the internal mode, followed by the external modes $\omega = m/n$, $n = 5$, $m = 4, 6, 2, \dots$

4. Hopf Bifurcation of the internal mode.

4.1. Two-time scales. We use the method of multiple scales to analyze the oscillatory solutions that appear at the Hopf bifurcation points. For the uncoupled lasers, oscillations decay on an $O(\epsilon)$ time scale, which suggests that we introduce the slow time $T = \epsilon t$; time derivatives become $\frac{d}{dt} = \frac{\partial}{\partial t} + \epsilon \frac{\partial}{\partial T}$. We analyze the nonlinear problem using perturbation expansions in powers of $\epsilon^{1/2}$, e.g., $x_j(t) = \epsilon^{1/2} x_{j1}(t, T) + \epsilon x_{j2}(t, T) + \dots$; the relevant nonlinear terms and the slow-time derivative then balance at $O(\epsilon^{3/2})$. Finally, for simplicity we set $\beta = 1$ indicating identical lasers; however, relaxing this assumption to nearly identical lasers ($\beta = 1 + O(\epsilon)$) does not qualitatively change the results.

We now consider the effect of the two-time scale assumption on the delay term. With the additional slow time, the delay term becomes

$$(4.1) \quad y_j(t - \tau) \rightarrow y(t - \tau, T - \epsilon\tau).$$

If $\delta_j \ll 1$, then consideration of the delay term is postponed until higher order and appears as part of the solvability condition for the slowly varying amplitude. However, if $\delta_j = O(1)$, then the leading-order problem will contain the delay term and analytical progress is much more difficult.

If $\tau \gg O(1/\epsilon)$ (large delay), then $\epsilon\tau = O(1)$ and the delay term must be retained in the slow argument. However, if $\tau = O(1)$, then the slow argument can be expanded as [21]

$$(4.2) \quad y_j(t - \tau) = y_j(t - \tau, T) - \epsilon\tau \frac{\partial}{\partial T} y_j(t - \tau, T) + \dots$$

Now the delay of the slow argument is postponed to higher order. We shall see that this leads to simpler slow-evolution equations for $\delta \ll 1$ (see Eq. (4.5)), and is necessary to make any progress at all for $\delta = O(1)$ (see Sec. 5).

It should be noted that care must be taken when using a series expansion of a delay term in a differential equation. The Taylor series may itself be justified but doing so can change the stability of the differential equation. A simple example is given in

[30], while [31, 32] provide more theoretical discussions concerning restrictions on the size of the delay. In our presentation we will check the validity of our approximations by comparing our analytical and numerical results.

4.2. Bifurcation equation. From the linear-stability analysis, we know that the first bifurcation will be to the internal mode with $\omega \approx 1$ when $\Delta = \delta_1 \delta_2 = O(\epsilon^2)$ (we assume that $\tau_s \neq n\pi$, n even, and thus do not consider the case of the double-Hopf bifurcation). We present the case that both coupling constants are of the same order $\delta_j = \epsilon d_j$. However, as long as $\Delta = O(\epsilon^2)$ the bifurcation results are qualitatively the same.

Proceeding with the multiple-scale analysis, we find that at the leading order, $O(\epsilon^{1/2})$, we obtain the solutions

$$(4.3) \quad y_{j1}(t, T) = B_j(T)e^{it} + c.c., \quad x_{j1}(t, T) = iB_j(T)e^{it} + c.c.,$$

which exhibit oscillations with radial frequency 1 on the t time scale. To find the slow evolution of $B_j(T)$, we must continue the analysis to $O(\epsilon^{3/2})$. Then, to prevent the appearance of unbounded secular terms, we determine ‘‘solvability conditions’’ for the $B_j(T)$. Due to the scalings of δ_j and y_j , the delay terms $\delta_j y_j(t - \tau_j, T - \tau_{\epsilon, j})$ are $O(\epsilon^{3/2})$ and contribute to the solvability condition. The final result is

$$(4.4) \quad \frac{\partial B_j}{\partial T} = -\frac{a_j}{2} B_j(T) - \frac{i}{6} |B_j(T)|^2 B_j(T) + \frac{i}{2} d_k B_k(T - \tau_{\epsilon, k}) e^{-i\tau_k},$$

$j, k = 1, 2$, $j \neq k$, and where $\tau_{\epsilon, k} = \epsilon \tau_k$. The effect of the delay in the slow time appears explicitly in the delay terms $B_k(T - \tau_{\epsilon, k})$. The delay in the fast time has resulted in the exponential terms $e^{-i\tau_k}$. Eq. (4.4) is valid for arbitrary values of the delay (we have not simplified the delay term $B_k(T - \tau_{\epsilon, k})$). However, according to Eq. (4.2), if $\tau = O(1)$, then $\tau_{\epsilon, k} = O(\epsilon)$ and delay in the slow time is postponed until higher order. This results in a simpler solvability condition where the delay in the slow time does not appear.

$$(4.5) \quad \frac{\partial B_j}{\partial T} = -\frac{a_j}{2} B_j - \frac{i}{6} |B_j|^2 B_j + \frac{i}{2} d_k B_k e^{-i\tau_k}, \quad j, k = 1, 2, \quad j \neq k.$$

Periodic solutions to the original laser equations, Eqs. (2.4), correspond to T -independent solutions to the solvability conditions. The conditions are the same for both Eqs. (4.4) and (4.5) because the delay terms in Eq. (4.4) become constants. The full T -dependent solvability conditions, including delay, are required only to analyze the stability of the periodic solutions.

To determine the amplitude and phase of the periodic solutions, we let $B_j(T) = R_j(T)e^{i\theta_j(T)}$, define the phase difference $\psi = \theta_2 - \theta_1$ and set the time derivatives to zero. We obtain

$$(4.6) \quad \begin{aligned} 0 &= -a_1 R_1 - d_2 R_2 \sin(\psi - \tau_2), \\ 0 &= -a_2 R_2 + d_1 R_1 \sin(\psi + \tau_1), \\ 0 &= -\frac{1}{3}(R_2^2 - R_1^2) + d_1 \frac{R_1}{R_2} \cos(\psi + \tau_1) - d_2 \frac{R_2}{R_1} \cos(\psi - \tau_2). \end{aligned}$$

We find that

$$(4.7) \quad \tan(\psi) = \frac{a_2 d_2 S_2 \sin(\tau_2) - a_1 d_1 S_1 \sin(\tau_1)}{a_2 d_2 S_2 \cos(\tau_2) + a_1 d_1 S_1 \cos(\tau_1)},$$

where $S_1 = R_1^2$ and $S_2 = R_2^2$ and the amplitudes are found from the implicit equations

$$(4.8) \quad \begin{aligned} a_2^2 d_2^2 S_2^2 + a_1^2 d_1^2 S_1^2 + 2a_1 a_2 d_1 d_2 \cos(\tau_s) S_1 S_2 - d_1^2 d_2^2 \sin^2(\tau_s) S_1 S_2 = 0 \\ d_1 d_2 \sin(\tau_s) S_2 (S_1 - S_2) + 3d_1 d_2 \cos(\tau_s) (a_2 - a_1) S_1 S_2 \\ + 3(a_1 d_1^2 S_1^2 - a_2 d_2^2 S_2^2) = 0. \end{aligned}$$

Of particular note is that just as in the linear-stability analysis, the amplitudes of the periodic solutions depend on the sum of the delays $\tau_s = \tau_1 + \tau_2$. This corresponds to the effective round-trip time of information from laser-j returning to laser-j.

In App. A we present explicit solutions of Eq. 4.8 that specify $S_j = R_j^2$ as a function of the parameters and the delay τ_s . The expressions are rather complicated but are easily evaluated numerically. To obtain simpler expressions, we consider $\tau_s = (n + \xi)\pi$, where $\xi \ll 1$ and n an odd integer. That is, we tune the delay time τ_s to be near one of the minimums of the neutral stability curves in Fig. 3.2. The bifurcation equation is

$$(4.9) \quad R_2^2 = 3(a_1 + a_2) \frac{\sqrt{D_1}}{D_2} + \xi Z_{21} + O(\xi^2),$$

where

$$(4.10) \quad D_1 = \frac{d_1 d_2}{a_1 a_2} - 1, \quad D_2 = \frac{a_2 d_2}{a_1 d_1} - 1,$$

and Z_{21} is specified in App. A.

We compare the results of numerically computed bifurcation diagrams [33] and our analytical results in Figs. 4.1-4.3. In Figs. 4.1 and 4.3, $\tau_s = 5\pi$ and 53π , respectively, and hence $\xi = 0$ in Eq. (4.9). The analytical bifurcation equation describes the numerical results quite well even for d_2 far away from the bifurcation point. An expansion of Eq. (4.9) near the bifurcation point shows that

$$(4.11) \quad R_2 \sim (\Delta - \Delta_H)^{1/4}, \quad \Delta = \delta_1 \delta_2.$$

We also note that Eq. (4.9) is identical to the bifurcation equation we derived in [2] for two coupled lasers with opposite sign coupling. The coupled laser equations in [2] are identical to Eq. (2.4) except that in [2]: (i) there is no delay such that the coupling is instantaneous and (ii) we allowed the sign of one of the coupling constants to be positive. Near the bifurcation point, the small-amplitude periodic oscillations are nearly harmonic as indicated by Eq. (4.3). Thus, a positive coupling constant corresponds to an effective phase shift of half the period or, more generally, a phase shift of $\tau_s = n\pi$ (see App. B). Thus, we expect that when τ_s is tuned to the minimum of the neutral stability curves in Fig. 3.2, the bifurcation equations of the two cases should be equivalent.

In Fig. 4.2 we show the case when $\xi \neq 0$. Here we have tuned the delay τ_s to be to the right of the minimum with $\tau_s = (5 + 0.1)\pi$. The dashed curve is the result of numerically evaluating the full bifurcation equations, Eqs. (4.8). The solid curve is the approximation Eq. (4.9) and it shows very good agreement with the numerical results. In general, we maintain good agreement as we tune τ_s away from the minimum up to $\tau_s = (n \pm 0.15)\pi$, n odd. The full bifurcation equation, Eq. (4.8), where we have not made any assumption on the delay, maintains good agreement out to at least $\tau_s = (n \pm 0.4)\pi$; beyond that however, it loses fidelity as we approach the double-Hopf bifurcations at $\tau_s = (n \pm 1)\pi$ ($\tau_s = n\pi$, n even).

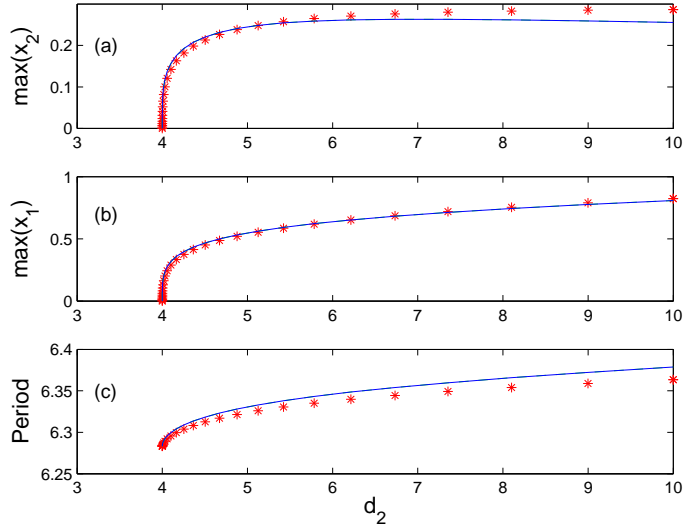


FIG. 4.1. *Internal mode, $n = 5$ with $\tau_1 = \tau_2 = n\pi/2$, and $\epsilon = 0.01$. Numerical data points indicated by *. The solid curve is the bifurcation equation determined by Eqs. (A.6)-(A.8) for $\xi = 0$, or Eqs. (A.1)-(A.5). Because $\tau_s = \tau_1 + \tau_2 = n\pi$, $\xi = 0$ so the bifurcation equations are equivalent ($d_1 = 1, a_1 = a_2 = 2, b = 1, \beta = 1$).*

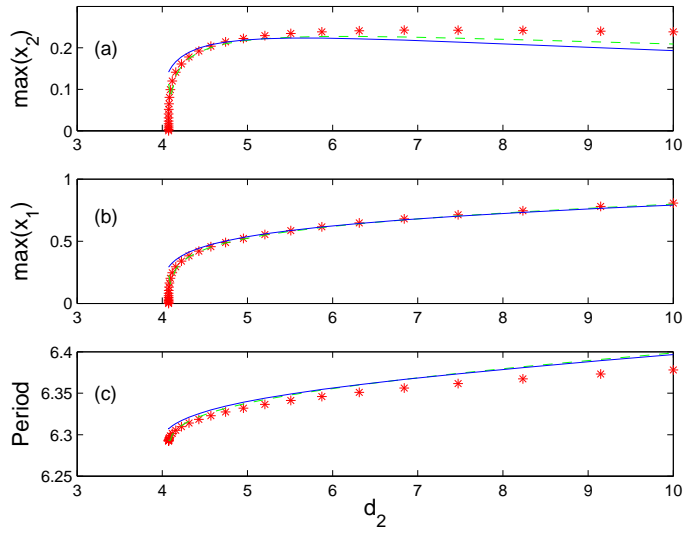


FIG. 4.2. *Same as Fig. 4.1 ($n = 5$) except that $\tau_1 = \tau_2 = (n + 0.1)\pi/2$. Thus, $\tau_s = (n + 0.1)\pi$, $\xi = 0.1\pi$ and the delay is tuned to the right of the minimum of the neutral-stability curve. The solid curves are the approximate bifurcation equations based on $\xi \ll 1$ given by Eqs. (A.6)-(A.8). The dashed curves are the more general bifurcation equations given by Eqs. (A.1)-(A.5). All other parameters are the same as in Fig. 4.1.*

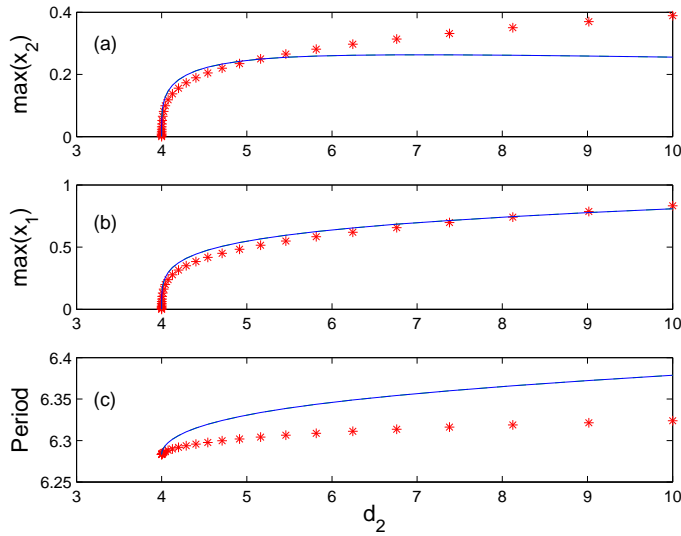


FIG. 4.3. Same as Fig. 4.1 except that $n = 53$.

Finally, we note that the first correction to the bifurcation equation Eq. (4.9) is linear in ξ . Thus, the bifurcation equation is not symmetric about the minimums of the neutral-stability curves; that is, the amplitude will be larger on one side of the minimum than the other for a given perturbation of Δ above the minimum.

4.3. Small-coupling resonance. The bifurcation equation Eq. (4.9) is singular when its denominator is zero ($D_2 = 0$), or

$$(4.12) \quad \Delta = \Delta_S \equiv \frac{a_1}{a_2} \delta_1^2$$

($\Delta = \delta_1 \delta_2$). If the parameters are such that the singular point is before the Hopf point, $\Delta_S < \Delta_H$, then the singularity can be ignored because the vanishing denominator will not occur when periodic solutions exist for $\Delta > \Delta_H$. However, if $\Delta_S > \Delta_H$, the bifurcation equation will exhibit the pole-type singularity. Near the singular point, the bifurcation equation predicts that the amplitude of the oscillations will become large corresponding to a resonance. The condition that $\Delta_S > \Delta_H$ corresponds to $\delta_1^2 > \epsilon^2 a_2^2$. Thus, in laser-2 the increase in the population inversion provided by pump coupling is greater than the effective losses. In [2], when the lasers were coupled without delay, we investigated this resonance in detail and the bifurcation equation matched the result of simulations very well. For the present case with delay coupling, however, we find that there are some dramatic differences.

In Fig. 4.4a, we compare the analytical and numerical bifurcation branches. For $d_1 = 2.3$, the bifurcation equation predicts a strong resonance peak. The numerical data for $d_1 = 2.3$ (*) exhibits a small resonance peak and there is good agreement between the analytical and numerical curves both before and after the singularity. In Fig. 4.4b we increase d_1 from 3.0 to 4.5 to follow the deformation of the bifurcation branch from an isolated resonance peak to a curve that forms a loop before continuing to higher values of d_1 ; this folding of the bifurcation branch is new to the system with delay and was not observed in [2]. We want to make clear that the bifurcation branch

is *not* intersecting itself. The apparent intersection results from projecting the full bifurcation curve of d_1 versus (x_1, y_1, x_2, y_2) , which does not intersect, onto the (d_1, x_2) plane.

Because the multiple-scale method is a local analysis and we assumed small-amplitude solutions, it is not unexpected that the analytical and numerical results match well near the bifurcation point. Similarly, in the vicinity of the resonance peak, the amplitude of the solutions becomes $O(1)$ and so it is not surprising that the analytical results fail to match the numerical results. That said, in our previous work with coupled lasers without delay [2], the analytically determined bifurcation equation matched the numerically computed resonance peak throughout the parameter range, i.e., even for $O(1)$ amplitudes; that was a bit surprising. We can surmise that in the present case it is the folding of the bifurcation branch that causes the mismatch. It may be that if we continued our analysis to higher order and derived additional nonlinear corrections to the bifurcation equation, we might better describe the folded branch. This would be a non-trivial and tedious calculation; but without doing so our supposition remains speculation. In [2] we used a different asymptotic method better suited to analyzing periodic solutions with $O(1)$ amplitudes with only partial success. Its application to the present problem with delay would be quite complicated and we have not made the attempt.

In Fig. 4.4b we increase d_1 to 5.0 and see that there is qualitative change in the bifurcation branch; there is no longer a loop, and the bifurcation branch continues to negative values of d_1 . In Fig. 4.4b we see that the change in the nature of the bifurcation curve appears quite abruptly at a critical value of d_1 . Typically, one expects smooth folding and unfolding of bifurcation branches as a parameter is changed [34]. In the present case, we have not been able to isolate an interval of d_1 over which such an unfolding might occur. To our knowledge, such a discontinuous unfolding of a branch of solutions in a bifurcation diagram has not been previously described.

Finally, if d_1 is increased further the bifurcation branch folds back and continues for positive d_2 ; there also appear to be secondary bifurcations but we have not explored these in any detail. We mention that as the delay τ_s increases, or as ϵ increases, the effect of the singularity is diminished. Conversely, with reduced values of ϵ , the bifurcation branch may exhibit more complicated turns and folds. It is intuitively understandable that increasing the damping (ϵ) will diminish any type of resonance phenomena. The role of the longer delay is unclear.

5. Hopf Bifurcation of the external modes. In this section, we describe the external modes that emerge via Hopf bifurcations as the coupling is increased. We fix $\delta_1 = O(1)$ and use δ_2 as the bifurcation parameter with $\delta_2 = \delta_{20} + \epsilon\delta_{22} + \dots$. We again have the slow time $T = \epsilon t$ and the perturbation expansion of x and y in powers of $\epsilon^{1/2}$. The multiple-scale analysis is more complicated because the $O(1)$ couplings result in a leading-order problem that contains the delay terms. Due to the two time scales, the delay terms are of the form $\delta_j y_j(t - \tau_j, T - \epsilon\tau_j)$. To make analytical progress we need to remove the slow delay from the leading-order problem. This requires that we assume $\epsilon\tau_j \ll 1$ such that by using Eq. (4.2) the slow delay is postponed to higher order. We then have a restriction on the size of the delay such that $\tau = o(1/\epsilon)$. Thus, we find that our results fit well with the external modes corresponding to the case $\tau_s = 5\pi$, Fig. 3.1b, but are inaccurate in the case $\tau_s = 53\pi$, Fig. 3.1c. Finally, to simplify the presentation, we consider the case of equal delays $\tau_1 = \tau_2 = \tau$, such that $\tau_s = 2\tau$; analysis of the general case with unequal delays can be carried out in the same way.

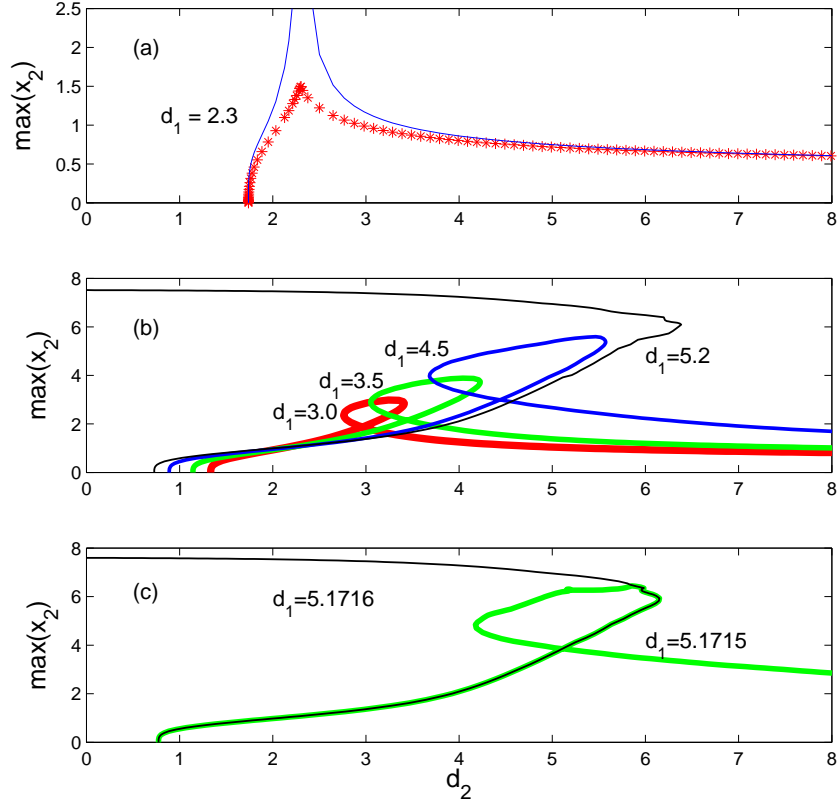


FIG. 4.4. *Internal mode, $n = 1$ with $\tau_s = n\pi$. (a) The solid curve is the predicted bifurcation branch from Eqs. (A.6) when d_1 is tuned such that the singularity in the bifurcation equation occurs after the Hopf bifurcation. The * are the numerical bifurcation data for $d_1 = 2.3$. (b) Numerical bifurcation branches as they deform between $d_1 = 3.0$ and $d_1 = 5.2$. (c) There is a critical value of d_1 , where on either side of the critical value the bifurcation branch has a loop and proceeds to higher values of d_1 , or bends back without a loop to negative values of d_1 . All other parameters are the same as in Fig. 4.1*

5.1. Leading order. The leading order $O(\epsilon^{1/2})$ problem is

$$(5.1) \quad \frac{\partial}{\partial t} X_1(t, T) = L \cdot X_1(t, T) - D \cdot X_1(t - \tau, T),$$

where

$$(5.2) \quad L = \begin{pmatrix} 0 & -1 & 0 & 0 \\ 1 & 0 & 0 & 0 \\ 0 & 0 & 0 & -1 \\ 0 & 0 & 1 & 0 \end{pmatrix}, \quad D = \begin{pmatrix} 0 & 0 & 0 & \delta_{20} \\ 0 & 0 & 0 & 0 \\ 0 & \delta_1 & 0 & 0 \\ 0 & 0 & 0 & 0 \end{pmatrix},$$

$$\text{and } X_1(t, T) = \begin{pmatrix} x_{11}(t, T) \\ y_{11}(t, T) \\ x_{21}(t, T) \\ y_{21}(t, T) \end{pmatrix}.$$

We look for oscillatory solutions of the form $X_1(t, T) = U_1 B(T) \exp(i\omega t)$, where $B(T)$ is a slowly varying scalar amplitude (to be determined from a solvability condition at $O(\epsilon^{3/2})$). U_1 is a vector that is determined by substituting our ansatz into Eq. (5.1) to obtain

$$(5.3) \quad 0 = J \cdot U_1 \quad \text{where} \quad J = \begin{pmatrix} -i\omega & -1 & 0 & -\delta_{20}e^{-i\omega\tau} \\ 1 & -i\omega & 0 & 0 \\ 0 & -\delta_1 e^{-i\omega\tau} & -i\omega & -1 \\ 0 & 0 & 1 & -i\omega \end{pmatrix}.$$

For a nonzero solution U_1 , we require $\det J = 0$. This results in the same condition obtained from the leading-order linear-stability problem; specifically,

$$(5.4) \quad (1 - \omega^2)^2 - \delta_1 \delta_{20} e^{-i2\omega\tau} = 0.$$

Thus, we have that

$$(5.5) \quad \omega = \frac{m\pi}{2\tau}, \quad m = \text{even, positive integer.}$$

For later reference it will be useful to note that

$$(5.6) \quad e^{-i2\omega\tau} = 1, \quad \text{and} \quad e^{-i\omega\tau} = \pm 1 = \nu_m,$$

where $\nu_m = +1$ if $m/2$ is odd (e.g. $m = 2, 6, \dots$) and $\nu_m = -1$ if $m/2$ (e.g. $m = 4, 8, \dots$) is even. Finally, we find that

$$(5.7) \quad U_1 = \begin{pmatrix} i\omega \\ 1 \\ i\omega u_1 \\ u_1 \end{pmatrix} \quad \text{where} \quad u_1 = \nu_m \sqrt{\frac{\delta_1}{\delta_{20}}}.$$

5.2. Second order. At $O(\epsilon)$ the problem is

$$(5.8) \quad \frac{\partial}{\partial t} X_2(t, T) = L \cdot X_2(t, T) - D \cdot X_2(t - \tau, T) + F_2,$$

$$\text{where} \quad F_2 = \begin{pmatrix} 0 \\ x_{11} y_{11} \\ 0 \\ x_{21} y_{21} \end{pmatrix}.$$

Because the homogeneous problem is the same as the $O(\epsilon^{1/2})$ problem we can, without loss of generality, set the homogeneous solution to 0. The inhomogeneous term F is proportional to $\exp(i2\omega t)$ so that the solution is

$$(5.9) \quad X_2(t, T) = B(T)^2 U_2 e^{i2\omega t} + c.c.$$

where U_2 is specified in App. C.

5.3. Third order . At $O(\epsilon^{3/2})$ we find the solvability condition that determines the slow-evolution equation for $B(T)$. The $O(\epsilon^{3/2})$ problem is

$$(5.10) \quad \frac{\partial}{\partial t} X_3(t, T) = L \cdot X_3(t, T) - D \cdot X_3(t - \tau, T) + F_3,$$

where

$$(5.11) \quad F_3 = \begin{pmatrix} -a_1 x_{11} - \delta_{22} y_{21}(t - \tau, T) + \delta_{20} \tau \frac{\partial}{\partial T} y_{21}(t - \tau, T) - \frac{\partial}{\partial T} x_{11} \\ x_{12} y_{11} + x_{11} y_{12} - \frac{\partial}{\partial T} y_{11} \\ -a_2 x_{21} + \delta_1 \tau \frac{\partial}{\partial T} y_{11}(t - \tau, T) - \frac{\partial}{\partial T} x_{21} \\ x_{22} y_{21} + x_{21} y_{22} - \frac{\partial}{\partial T} y_{21} \end{pmatrix}.$$

The vector F_3 has terms proportional to $\exp(i\omega t)$ and $\exp(i2\omega t)$ and the former will lead to solutions of the form $(U_3 + V_3 t) \exp(i\omega t)$. The secular terms $V_3 t$ must be eliminated to prevent unbounded solutions for large t , which implies that a solvability condition must be imposed on F_3 . The solvability condition is formulated as follows: We look for a solution to Eq. (5.10) of the form $X_3 = U \exp(i\omega t)$ and at the same time identify the terms F in F_3 proportional to $\exp(i\omega t)$. We then obtain a algebraic system of equations for the vector U as

$$(5.12) \quad 0 = J \cdot U + F,$$

where

$$(5.13) \quad F = \begin{pmatrix} (-i\omega a_1 - \delta_{22} u_1 \nu_m) B - (i\omega - \delta_{20} \tau u_1 \nu_m) B_T \\ i\omega(u_{22} - 1) |B|^2 B - B_T \\ -i\omega a_2 u_1 B - (i\omega - \delta_1 \tau \nu_m) B_T \\ i\omega u_1 (u_{24} - u_1^2) |B|^2 B - u_1 B_T \end{pmatrix}.$$

For U to have a non-zero solution, the Fredholm Alternative requires that $V^H \cdot F = 0$, where V is the solution to $J^H \cdot V = 0$ (the superscript H refers to Hermitian). We find that $V^H = (u_1, i\omega u_1, 1, i\omega)$, and the resulting condition for the amplitude $B(T)$ is

$$(5.14) \quad \frac{\partial B}{\partial T} = (p_l + iq_l) B + (p_n + iq_n) B |B|^2,$$

where $p_{l,n}$ and $q_{l,n}$ are given in App. C.

5.4. Bifurcation equation. To analyze the solvability condition given by Eq. (5.14), we let $B(T) = R(T) e^{i\theta(T)}$ to obtain

$$(5.15) \quad \frac{\partial R}{\partial T} = (p_l + p_n R^2) R,$$

$$(5.16) \quad \frac{\partial \theta}{\partial T} = q_l + q_n R^2.$$

The equation for θ determines the frequency correction as a function of the amplitude. The bifurcation equation is determined by considering steady-state solutions to the equation for R , and we find that

$$(5.17) \quad R^2 = -\frac{p_l}{p_n} = -\left(\frac{|\delta_1|}{r_2 \omega^2 |1 - \omega^2|} \right) \left[\delta_1 \delta_{22} - \frac{2\omega^2 (a_1 + a_2)}{\tau} \right].$$

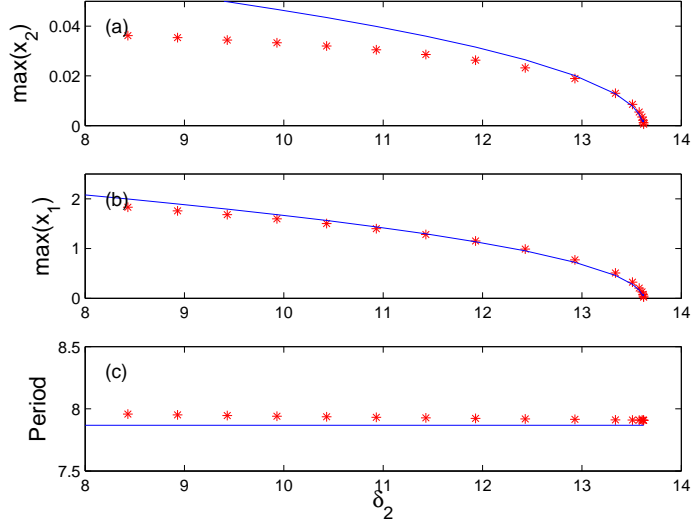


FIG. 5.1. *External mode, $n = 5$, $m = 4$ with $\tau_1 = \tau_2 = n\pi/2$, and $\epsilon = 0.01$. Numerical data points are indicated by *. The solid curve is the asymptotic approximation based on Eq. (5.17). ($d_1 = 1, a_1 = a_2 = 2, b = 1, \beta = 1$)*

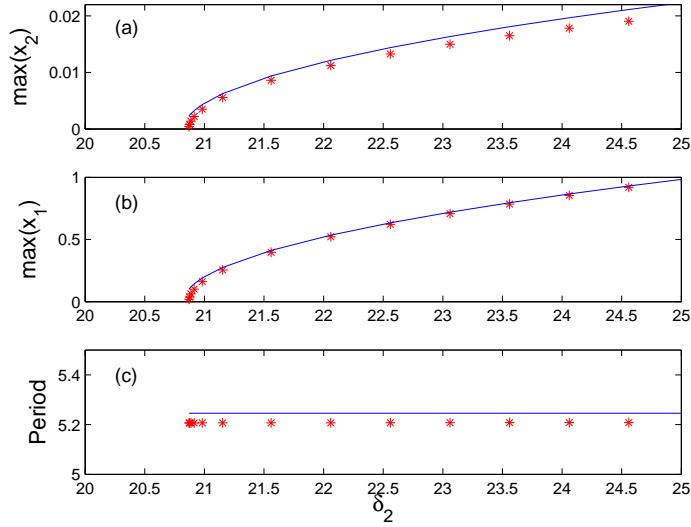


FIG. 5.2. *Same as Fig. 5.1 except $m = 6$. All other parameter values are the same.*

The onset of oscillations occurs when $R = 0$ and determines δ_{22} at the Hopf bifurcation point; this result matches exactly that obtained in the linear-stability analysis.

In Figs. 5.1 and 5.2, we compare the bifurcation equation Eq. (5.17) to the numerically computed result. In each figure we have $\tau_s = 5\pi = O(1)$ (see Figs. 4.1 and 4.2 for analysis of the internal mode). In Fig. 5.1 the external mode corresponds to

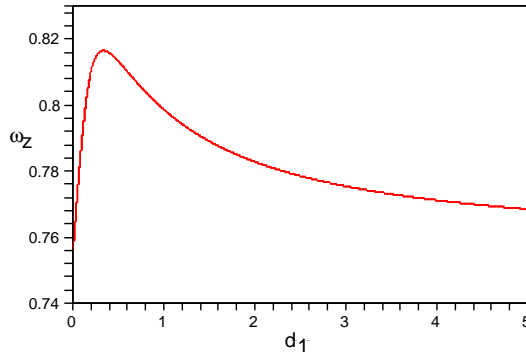


FIG. 5.3. Upper bound on the value of ω as a function of d_1 giving a sign change for parameter r_2 in Eq. (C.5).

$m = 4$ and its direction of bifurcation is subcritical. In Fig. 5.2 we have $m = 6$ and the bifurcation is supercritical. In each case, there is good agreement between the numerical and analytical result local to the bifurcation point, where the multiple-scale analysis' validity is strongest.

The direction of bifurcation (super- or subcritical) in Eq. (5.17) is controlled by the sign of the constant r_2 , which is given in Eq. (C.5). Analysis of r_2 shows that $r_2 > 0$ in the interval $\sqrt{2/5} < \omega < \omega_z(d_1)$, where $\omega_z(d_1)$ is shown in Fig. 5.3 (the lower bound is a zero of the denominator of r_2 , while the upper bound is the sole real zero of the numerator). Thus, for external modes with frequencies within this interval, the bifurcation will be subcritical; this is the case for the external mode in Fig. 5.1. For all other modes $r_2 < 0$ and the direction of the bifurcation will be supercritical.

For reference, in Fig. 5.4 we show the bifurcation diagrams of the internal mode ($\omega \approx 1$) and the external modes ($\omega = m/n$, $m = 4$ and $m = 6$) for the case $n = 5$; that is, we have combined the bifurcation diagrams of Figs. 4.1, 5.1 and 5.2. The subcritical bifurcation for the external mode $m = 4$ folds to provide an interval of hysteresis. The bifurcation branches are projections onto planes so that the intersections of the curves are not relevant. The periodic solutions corresponding to the external modes are unstable as they bifurcate from the unstable branch of steady-state solutions. The internal mode is stable until $d_2 \approx 59$, when a period-doubling sequence to chaos begins.

Finally, we note that for the external modes

$$(5.18) \quad R \sim [\Delta - \Delta_H]^{1/2}.$$

The amplitude of the external modes varies as the square root of the distance from the bifurcation point. In contrast, the internal mode varies as $1/4$ the power of the deviation.

6. Discussion. We have analyzed the output of two mutually coupled lasers, where the light intensity deviations from steady state modulated the pump of the other laser. The coupling strength in one direction is held fixed, while we examine the effect of increasing the coupling strength in the other direction. The signal-propagation time through the optical fiber and the electronic circuit causes a delay leading to a model that is a system of delay-differential equations. Linear-stability analysis finds that the

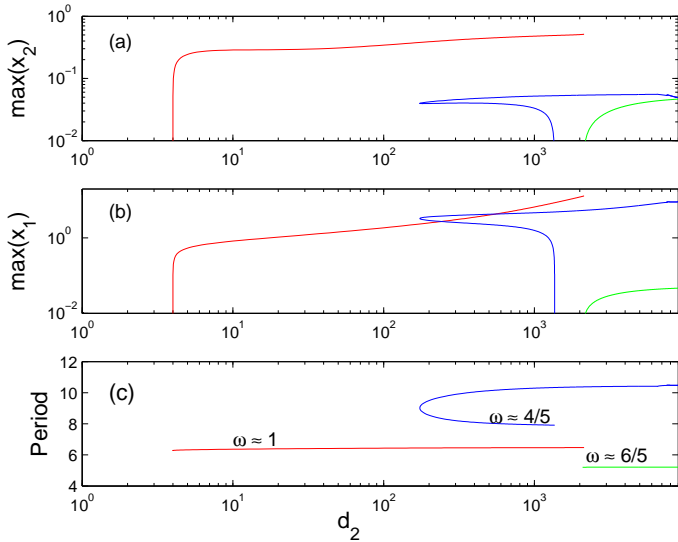


FIG. 5.4. Numerically computed bifurcation diagrams, both internal and external modes, for $n = 5$ and $\tau_s = n\pi$. The left-most branch corresponds to the internal mode shown in Fig. 4.1; periodic solutions are stable until $d_2 \approx 59$, when there is a period-doubling bifurcation. The middle and right-most branches are the continuation of the external modes shown in Fig. 5.1 ($m = 4$) and Fig. 5.2 ($m = 6$), respectively; periodic solutions are unstable along these branches ($\epsilon = 0.01, d_1 = 1, a_1 = a_2 = 2, b = 1, \beta = 1$).

steady-state solution becomes unstable at a Hopf bifurcation; we call the resulting periodic solution the internal mode because it oscillates at the laser’s relaxation-oscillation frequency. As the coupling is increased, subsequent instabilities occur with frequencies determined by the round-trip delay time $\omega_e = m\pi/\tau_s$, $m = 2, 4, 6, \dots$; we call these periodic solutions external modes.

Using a multiple-scale analysis, we derive bifurcation equations for both the internal and external modes. We find that the amplitude of the internal mode increases with the $1/4$ -root of the deviation from the bifurcation point and is supercritical; i.e., $R \sim +(\Delta - \Delta_H)^{1/4}$. The amplitude of the external modes increase with the $1/2$ -root of the deviation and may be super- or subcritical; i.e., $R \sim \pm(\Delta - \Delta_H)^{1/2}$. Both the initial instability and the bifurcation results depend on the product of the coupling constants $\Delta = \delta_1\delta_2$. For the analysis of the internal mode, we assumed that both coupling constants were of the same relative size, $\delta_j = O(\epsilon)$. However, other scalings satisfy the Hopf condition, e.g., $\delta_1 = O(\epsilon^{1/2})$ and $\delta_2 = O(\epsilon^{3/2})$. We have found that this does not change the qualitative properties of the bifurcation.

We have focused our analysis on the onset of oscillatory instabilities and just beyond. We have not considered the stability of the internal and external modes as the coupling is increased further. However, numerical simulations indicated period-doubling bifurcations of individual modes as well as multimode behavior.

With independent control of the individual coupling strengths, we have observed an atypical resonance phenomena. As in our previous work on two mutually coupled lasers without delay [2], there is an interval of the coupling parameter δ_2 over which the amplitude of the oscillations becomes large; we have referred to this effect as a “resonance.” The bifurcation equation, Eq. (4.9), can describe the amplitude of

the oscillations for δ_2 above and below resonance. A singularity in the bifurcation equation indicates the existence of the resonance, but Eq. (4.9) does not describe the amplitude within the resonance well. The parametric form of the singularity indicates that physically, the coupling term provides an effective negative-damping that cancels with the lasers self-damping and hence provides a resonance effect.

What is different from the results in [2] is that the bifurcation branch folds with a change in the coupling parameter δ_1 ; in Figs. 4.4 we see that the resonance peak forms a loop in the (d_1, x_2) plane. We also find that instead of a smooth unfolding of the loop, there appears to be a critical value of the parameter d_1 where the folded portion of the bifurcation branch abruptly disappears. To our knowledge, such a discontinuous unfolding of a branch of solutions in a bifurcation diagram has not been previously described. We do not understand the mechanism or manner by which the abrupt change occurs, but this will be the focus of future work.

The application of multiple-scale perturbation techniques to DDEs is, to our knowledge, a relatively recent development [21]. For our analysis of the internal modes, the delay terms appeared only as part of the solvability condition; thus, the multiple-scale analysis was relatively straightforward. In contrast, for the external modes that bifurcate when the coupling constants are $O(1)$, the delay terms are included in the leading-order problem. However, by looking for periodic solutions we are able to continue the analysis and formulate a solvability condition. Finally, as mentioned in the text, multiple-scale expansion of the delay term in Eq. (4.2) amounts to a Taylor series expansion that, while it may be justified in and of itself, can lead to erroneous results for the DDE [30]. Thus, it is important to compare our analytical results to those from numerical simulations as an important check of the work.

As discussed in the introduction, the method of averaging has also been used to analyze the weakly-nonlinear characteristics of delay problems. Averaging and the multiple-scale technique will lead to a similar slow-time evolution equation for the amplitudes. However, the multiple-scale technique accounts for the delay in the slow time where averaging does not. Because we focused on the existence of periodic solutions, the slow-time delay is removed and both averaging and multiple-scales give equivalent results. However, stability of the periodic solutions, or the investigation of more complicated phenomena such as quasiperiodicity, would require the slow-delay from the multiple-scale analysis.

Finally, we finish with a discussion relating the results of our analysis to experimental results observed in [1] and [22]. The coupling circuit in the experimental system has two important characteristics. First, the signal is inverted, which results in the negative signs that appear in front of the coupling constants in Eq. (2.4). Second, the circuit acts as a low-pass filter that suppresses coupling of the relaxation-oscillations. We discuss the effect of each of these below.

The signal inversion of the coupling circuit results in negative coupling constants in Eq. (2.4). However, both the linear-stability and the leading-order bifurcation results depend on the product of the coupling constants $\Delta = \delta_1 \delta_2$. Thus, local to the Hopf bifurcation it does not matter if both δ_j are negative or both are positive. More generally, our results depend only on whether Δ is positive or negative, not on the signs of the individual coupling constants. This is effectively a symmetry result, because for small amplitudes the oscillations are nearly harmonic. This means a sign change is merely a phase shift. However, we have observed in numerical simulations that when the amplitudes become larger such that the intensity is pulsating, the symmetry is lost such that positive coupling results in different system output from

negative coupling.

As mentioned above, the optoelectronic coupling circuit in [1] and [22] acts as a low-pass filter on the coupling signal. We do not account for this in our model of the system (recently, Illing and Gauthier [35] have analyzed a DDE where they explicitly account for the bandlimited response of their feedback system). However, because our results address the linear and nonlinear dynamics of both the internal and external modes, we can make a comparison between theory and experiment.

The low-pass filter characteristic of the experimental coupling circuit attenuates the high-frequency relaxation-oscillations, corresponding to the internal mode. The result is that the experimental system oscillates at one of the low-frequency external modes. This is illustrated in Fig. 6.1, where we indicate the experimentally observed external mode with a (o) for different values of the delay. The (+) indicate the theoretical value of $\Delta_H(\omega)$ for a bifurcation to an external mode. Linear stability predicts that as the frequency increases the coupling strength, Δ_H , required for a Hopf bifurcation decreases (see also Fig. 3.1 for small ω). However, there is a filter-cutoff frequency ω_c such that the relaxation oscillations and higher-frequency external modes are attenuated and only the external modes with frequencies $\omega_e < \omega_c$ are observed.

For example, in [1] we observed oscillations with period equal to the round-trip delay time; specifically, $\omega = 2\pi/T = 2\pi/\tau_s$ corresponding to the external mode with $m = 2$. This indicates that the filter-cutoff frequency, ω_c , is such that $2\pi/\tau_s < \omega_c < 4\pi/\tau_s$. If ω_c was greater than $4\pi/\tau_s$ then we would have expected to observe the external mode with $m = 4$ because the value of the coupling at the Hopf-bifurcation point decreases as ω_e increases, i.e., it will bifurcate at a lower value of the coupling.

More recent experiments [22] confirm that with longer delays, external modes with $m > 2$ are exhibited; this is shown in the lower two plots in Fig. 6.1. That is, as the delay increases, the external modes with larger m will be below the cutoff frequency, $\omega_e = m\pi/\tau_s < \omega_c$. And it is always the mode with largest frequency, but still below cutoff, that is exhibited because $\Delta_H(\omega)$ is least for that frequency. Taking all five plots together, the experimental data suggest that the low-pass filter cutoff frequency is $\omega_c \approx 0.05$ because all of the observed modes have frequency less than ω_c . Finally, we add that it was observed in [1] that the amplitude of the oscillations followed a square-root power law as a function of the coupling. This is exactly as predicted by the bifurcation equation Eq. (5.17) for the external modes.

Our comparison between the theory and the experiment does have limitations. We do not know the detailed filter characteristics of the optoelectronic coupling circuit. It is known that the filter profile is most certainly not a step function but is instead frequency dependent; it depends on the properties of the optical cable, the electronic coupling circuit and the frequency response of the laser to the modulated pump. In addition, for large values of the delay the frequency difference between the external modes becomes very small and many external modes are excited at nearly the same value of the coupling. For these cases the linear stability theory may be insufficient to identify the mode that is observed in the experiments.

Acknowledgments. I.B.S acknowledges the support of the Office of Naval Research.

Appendix A. Amplitudes of periodic solutions.

$$(A.1) \quad R_2^2 = \frac{N}{D},$$

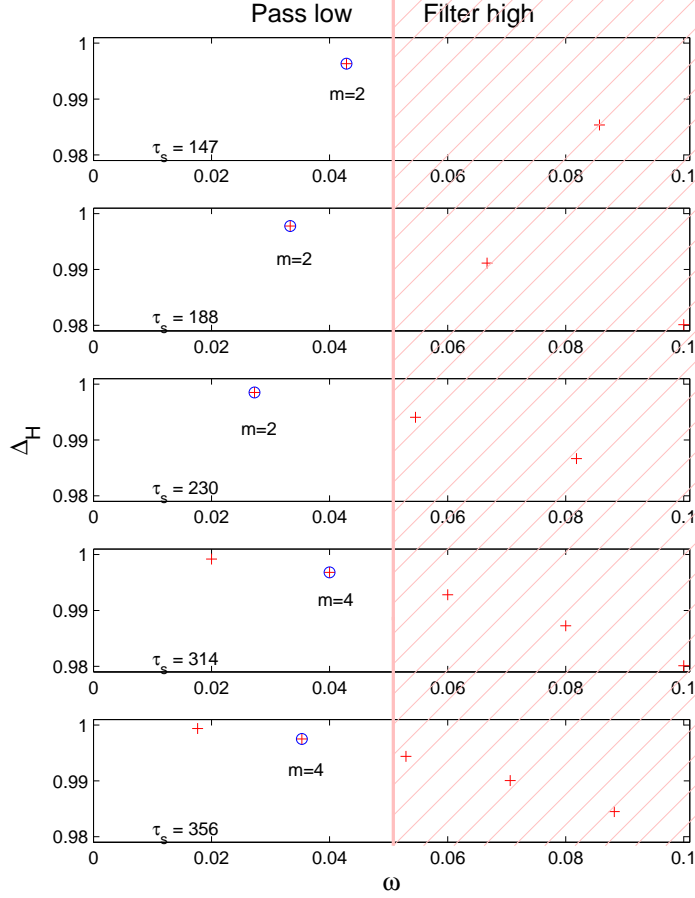


FIG. 6.1. For each value of delay, linear stability predicts a set of external modes with frequencies $\omega_e = m\pi/\tau_s$, m even, indicated by $+$. The frequencies of the external modes have been plotted on the linear-stability curve $\Delta_H(\omega)$ as in Fig. 3.1. External modes with higher frequency bifurcate first because $\Delta_H(\omega)$ is decreasing. For each value of the delay, the (\circ) indicates the specific external mode observed in experiment. All of the observed modes are less than a cutoff frequency due to the low-pass filter characteristic of the coupling circuit.

where

$$(A.2) \quad N = 3Q [a_1 d_1^2 d_2 \sin^2 \tau_s - a_1^2 d_1 (a_1 + a_2) \cos \tau_s] \\ - 3 a_1 d_1^3 d_2^2 \sin^3 \tau_s + 3 a_1^2 d_1^2 d_2 (3 a_2 + a_1) \sin \tau_s \cos \tau_s \\ + 6 a_1^3 a_2 d_1 (a_1 + a_2) \sin \tau_s,$$

$$(A.3) \quad D = Q \sin \tau_s [a_1^2 d_1 - d_1 d_2^2 \sin^2 \tau_s + 2 a_1 a_2 d_2 \cos \tau_s] \\ + d_1^2 d_2^3 \sin^4 \tau_s - 4 a_1 a_2 d_1 d_2^2 \cos \tau_s \sin^2 \tau_s - 4 a_1^2 a_2^2 d_2 \sin^2 \tau_s, \\ + 2 a_1^3 a_2 d_1 \cos \tau_s - a_1^2 d_1^2 d_2 \sin^2 \tau_s + 2 a_1^2 a_2^2 d_2$$

$$(A.4) \quad Q = \sqrt{d_1^2 d_2^2 \sin^2 \tau_s - 4 a_1 a_2 d_1 d_2 \cos \tau_s - 4 a_1^2 a_2^2},$$

and

$$(A.5) \quad R_1^2 = \frac{d_2}{2a_1^2 d_1} (d_1 d_2 \sin^2 \tau_s - 2 a_2 a_1 \cos \tau_s - Q \sin \tau_s) R_2^2.$$

When the delay is tuned to be near one of the minimums of the neutral stability curves, i.e., $\tau_s = m\pi + \xi$, $\xi \ll 1$, we have

$$(A.6) \quad \begin{aligned} R_2^2 &= Z_{20} + \xi Z_{21} + O(\xi^2), \\ Z_{20} &= 3(a_1 + a_2) \frac{\sqrt{D_1}}{D_2}, \\ Z_{21} &= \frac{3(D_1 + 1)}{2d_1^2 D_2^2} [D_1(a_2^3 + 3a_2^2 a_1) + (a_2 - a_1)(d_1^2 - a_2^2)], \\ D_1 &= \frac{d_1 d_2}{a_1 a_2} - 1, \\ D_2 &= \frac{a_2 d_2}{a_1 d_1} - 1. \end{aligned}$$

$$(A.7) \quad R_1^2 = \left(\frac{a_2}{d_1}\right)^2 (D_1 + 1) [Z_{20} + \xi(Z_{20} \sqrt{D_1} + Z_{21})] + O(\xi^2),$$

$$(A.8) \quad \omega = 1 - \epsilon \left(\frac{1}{6} Z_{20} + \frac{1}{2} a_2 \sqrt{D_1} \right) - \xi \epsilon \left[\frac{1}{6} Z_{21} + \frac{1}{4} a_2 (D_1 + 1) \right] + O(\xi^2).$$

Appendix B. Delay and opposite-sign coupling.

Consider a negative coupling constant such that

$$(B.1) \quad \frac{dx_1}{dt} \sim +\delta_2 y_2(t).$$

If y_2 is harmonic with frequency $\omega = 1$ and given by $y_2 = A \cos(t)$, then

$$(B.2) \quad \begin{aligned} \frac{dx_1}{dt} &\sim +\delta_2 A \cos(t), \\ &-\delta_2 A \cos(t - n\pi), \quad n \text{ an odd integer}, \\ &-\delta_2 A \cos(t - \tau_s), \end{aligned}$$

where $\tau_s = n\pi$ is the total ‘‘round-trip’’ or system-delay because the other coupling constant, δ_1 , is negative.

Appendix C. External modes: coefficients.

C.1. Second order: $O(\epsilon)$.

$$(C.1) \quad U_2 = \begin{pmatrix} i\omega(2u_{22} - 1) \\ u_{22} \\ i\omega(2u_{24} - u_1^2) \\ u_{24} \end{pmatrix}$$

and

$$(C.2) \quad u_{22} = -\frac{2\omega^2[1 - 4\omega^2 - \delta_1]}{(1 - 4\omega^2)^2 - \delta_1 \delta_{20}}, \quad u_{24} = -\frac{2\omega^2[u_1^2(1 - 4\omega^2) - \delta_1]}{(1 - 4\omega^2)^2 - \delta_1 \delta_{20}}.$$

C.2. Third order: $O(\epsilon^{3/2})$.

$$(C.3) \quad p_l = r_1[\delta_1 \delta_{22} \tau - 2\omega^2(a_1 + a_2)], \quad q_l = r_1 \left\{ \nu_m u_1 \omega [(a_1 + a_2) \frac{\tau}{\delta_{20}} + 2\delta_{22}] \right\}$$

$$(C.4) \quad p_n = r_1 r_2 \tau \nu_m \frac{\omega^2}{u_1} \delta_1, \quad q_n = r_1 r_2 2\omega^3,$$

$$(C.5) \quad r_1 = \frac{1}{2(\delta_1 \delta_{20} \tau^2 + 4\omega^2)}, \quad r_2 = \frac{\delta_1(\delta_1 + \delta_{20} + 4\omega^2) - (1 + u_1^2)(1 - 2\omega^2)(1 - 4\omega^2)}{(1 - 4\omega^2)^2 - \delta_1 \delta_{20}}$$

REFERENCES

- [1] M-Y Kim, R. Roy, J.L. Aron, T.W. Carr, and I.B. Schwartz. Scaling behavior of laser population dynamics with time-delayed coupling: Theory and experiment. *Phys. Rev. Lett.*, 94(8):088101, February 2005.
- [2] T.W. Carr, M.L. Taylor, and I.B. Schwartz. Negative-coupling resonances in pump-coupled lasers. *Physica D*, 215:152–163, 2006.
- [3] H. Yaska and H. Kawaguchi. Linewidth reduction and optical frequency stabilization of a distributed feedback laser by incoherent optical negative feedback. *Appl. Phys. Lett.*, 53:1360–1362, 1988.
- [4] R. Lang and K. Kobayashi. External optical feedback effects on semiconductor injection laser properties. *IEEE J. Quantum Electron.*, QE-16:347–355, 1980.
- [5] G.H.M. van Tartwijk and D. Lenstra. Semiconductor lasers with optical injection and feedback. *Quantum Semiclass. Opt.*, 7:87–143, 1995.
- [6] J. Javaloyes, P. Mandel, and D. Pieroux. Dynamical properties of lasers coupled face to face. *Phys. Rev. E*, page 036201, 2003.
- [7] H. Erzgräber, B. Krauskopf, and D. Lenstra. Compound laser modes of mutually delay-coupled lasers. *SIAM J. Appl. Dyn. Syst.*, 5(1):30–65, 2006.
- [8] R.D. Li, P. Mandel, and T. Erneux. Periodic and quasiperiodic regimes in self-coupled lasers. *Phys. Rev. A*, 41(9):5117–5126, May 1990.
- [9] D. Pieroux, T. Erneux, and K. Otsuka. Minimal model of a class-b laser with delayed feedback: Cascading branching of periodic solutions and period-doubling bifurcation. *Phys. Rev. E*, 50:1822–1829, 1994.
- [10] D.W. Sukow, A. Gavrielides, T. Erneux, M.J. Baracco, Z.A. Parmenter, and K.L. Blackburn. Two-field description of chaos synchronization in diode lasers with incoherent optical feedback and injection. *Proc. SPIE*, 5722:256–258, 2005.
- [11] R. Vicente, S. Tang, J. Mulet, C.R. Mirasso, and J.M. Liu. Dynamics of semiconductor lasers with bidirectional optoelectronic coupling: stability, route to chaos and entrainment. *Phys. Rev. E*, 70:046216, 2004.
- [12] R. Vicente, S. Tang, J. Mulet, C.R. Mirasso, and J.M. Liu. Synchronization properties of two self-oscillating semiconductor lasers subject to delayed optoelectronic mutual coupling. *Phys. Rev. E*, 73:047201, 2006.
- [13] D.V.R. Reddy, A. Sen, and G.L. Johnston. Driven response of time delay coupled limit cycle oscillators. *Com. in Nonlinear Sci. and Num. Simul.*, 8:493–518, 2003.
- [14] A.K. Sen and R.H. Rand. A numerical investigation of the dynamics of a system of two time-delay coupled relaxation oscillators. *Comm. Pure and Applied Math.*, 2:567–577, 2003.
- [15] S. Wirkus and R. Rand. The dynamics of two coupled Van der pol oscillators with delay coupling. *Nonlinear Dynamics*, 30:205–221, 2002.
- [16] D.V.R. Reddy, A. Sen, and G.L. Johnston. Time delay induced death in coupled limit cycle oscillators. *Phys. Rev. Lett.*, 80:5109–5112, 1998.
- [17] S.R. Campbell and D.L. Wang. Relaxation oscillators with time delay coupling. *Physica D*, 111:151–178, 1998.
- [18] S.G. Lee, S. Kim, and H. Kook. Synchrony and clustering in two and three synaptically coupled Hodgkin-Huxley neurons with delay. *Int. J. Bifurcation and Chaos*, 7:889–895, 1997.
- [19] M.K. Stephen Yeung and S.H. Strogatz. Time delay in the Kuromoto model of coupled oscillators. *Phys. Rev. Lett.*, 82(3):648–651, 1999.
- [20] N.B. Abraham, P. Mandel, and L. M. Narducci. Dynamical instabilities and pulsations in lasers. *Prog. Opt.*, 25:3–190, 1988.

- [21] D. Pieroux, T. Erneux, A. Gavrielides, , and V. Kovanis. Hopf bifurcation subject to a large delay in a laser system. *SIAM. J. Appl. Math.*, 61:966–982, 2000.
- [22] Min-Young Kim. *Delay induced instabilities in coupled semiconductor lasers and Mack-Glass electronic circuits*. PhD thesis, University of Maryland, 2005.
- [23] C. Chicone and Z.C. Feng. Synchronization phenomena for coupled delay-line oscillators. *Physica D*, 198(3–4):212–230, 2004.
- [24] D.V.R. Reddy, A. Sen, and G.L. Johnston. Time delay effects on coupled limit cycle oscillators at Hopf bifurcation. *Physica D*, 129:15–34, 1999.
- [25] F.T. Arecchi, G.L. Lippi, G.P. Poccioni, and J.R. Tredicce. Deterministic chaos in laser with injected signal. *Optics Comm.*, 51:308–314, 1984.
- [26] P. Mandel. *Theoretical Problems in Cavity Nonlinear Optics*. Cambridge Studies in Modern Optics. Cambridge University Press, New York, 1997.
- [27] I.B. Schwartz and T. Erneux. Subharmonic hysteresis and period-doubling bifurcations for a periodically driven laser. *SIAM J. Appl. Math.*, 54:1083–1100, 1994.
- [28] F. Rogister, D. Pieroux, M. Sciamanna, P. Megret, and M. Blondel. Anticipating synchronization of two chaotic laser diodes by incoherent optical coupling and its application to secure communications. *Opt. Commun.*, 207:295–306, 2002.
- [29] W. Govaerts, J. Guckenheimer, and A. Khibnik. Defining functions for multiple Hopf bifurcations. *SIAM J. Numer. Anal.*, 34(3):1269–1288, 1997.
- [30] R.D. Driver. *Ordinary and delay differential equations*. Springer-Verlag, New York, 1977.
- [31] R.D. Driver, D.W. Sasser, and M.L. Slater. The equation $x'(t) = ax(t) + b(t - \tau)$ with “small” delay. *The American Mathematical Monthly*, 80(9):990–995, 1973.
- [32] L.E. El’sgol’ts and S.B. Norkin. *Introduction to the theory and application of differential equations with deviating arguments*, volume 105 of *Mathematics in Science and Engineering*. Academic Press, New York, 1973. Translated by J.L. Casti.
- [33] K. Engelborghs, T. Luzyanina, and G. Samaey. DDE-BIFTOOL v.2.00 user manual: a Matlab package for bifurcation analysis of delay differential equations. Technical Report TW-330, Dept. of Computer Science, K.U.Leuven, Leuven, Belgium, 2001.
- [34] S. Wiggins. *Introduction to Applied Nonlinear Dynamical Systems*. Springer-Verlag, New York, 1990.
- [35] L. Illing and D.J. Gauthier. Hopf bifurcations in time-delay systems with band-limited feedback. *Physica D*, 210:180–202, 2005.